6-2012

Noncontact ultrasound imaging applied to cortical bone phantoms

John Bulman
Loyola Marymount University, jbulman@lmu.edu

K. S. Ganezer
California State University, Dominguez Hills

P. W. Halcrow
California State University, Dominguez Hills

Ian Neeson
VN Instruments Ltd.

Noncontact ultrasound imaging applied to cortical bone phantoms

J. B. Bulman
Department of Physics, Loyola Marymount University, Los Angeles, California 90045

K. S. Ganezer[a)]
Department of Physics, California State University Dominguez Hills, Carson, California 90747

P. W. Halcrow
Department of Physics, California State University Dominguez Hills, Carson, California 90747 and Department of Biology, California State University Dominguez Hills, Carson, California 90747

Ian Neeson
VN Instruments Ltd., 2-4501 Ferguson Dr., Elizabethtown, Ontario K6T 1A9, Canada

(Received 7 January 2011; revised 29 March 2012; accepted for publication 10 April 2012; published 15 May 2012)

Purpose: The purpose of this paper was to take the first steps toward applying noncontact ultrasound (NCU) to the tasks of monitoring osteoporosis and quantitative ultrasound imaging (QUS) of cortical bone. The authors also focused on the advantages of NCU, such as its lack of reliance on a technologist to apply transducers and a layer of acoustical coupling gel, the ability of the transducers to operate autonomously as specified by preprogrammed software, and the likely reduction in statistical and systematic errors associated with the variability in the pressure applied by the clinician to the transmitting transducer that NCU might provide. The authors also undertook this study in order to find additional applications of NCU beyond its past limited usage in assessing the severity of third degree burns.
Methods: A noncontact ultrasound imaging system using a pair of specially designed broadband, 1.5 MHz noncontact piezoelectric transducers and cortical bone phantoms, were used to determine bone mineral density (BMD), speed of sound (SOS), integrated response (IR), and ultrasonic transmittance. Air gaps of greater than 3 cm, two transmission and two reflection paths, and a digital signal processor were also used in the collection of data from phantoms of nominal mass densities that varied from 1.17 to 2.25 g/cm^3 and in bone mineral density from 0 to 1.7 g/cm^3.
Results: Good correlations between known BMD and measured SOS, IR, and transmittance were obtained for all 17 phantoms, and methods for quantifying and minimizing sources of systematic errors were outlined. The BMD of the phantom sets extended through most of the *in vivo* range found in cortical bone. A total of 16–20 repeated measurements of the SOS, thickness, and IR for the phantom set that were conducted over a period of several months showed a small variation in the range of measurements of $\pm 1\%$–2%. These NCU data were shown to be in agreement with similar results using contact ultrasound to be within 1%–2%. Transmittance images of cortical bone phantoms showed differences in the nominal overall BMD values of the phantoms that were large enough to be distinguished by a visual examination. A list of possible sources of errors in quantitative NCU was also included in this study.
Conclusions: The results of this paper suggest that NCU might find additional applications in medical imaging, beyond its original and only previous usage in assessing third degree burns. The fact that the authors' phantom measurements using conventional, gel coupled ultrasound are in agreement with those obtained with NCU demonstrates that in spite of large additional levels of attenuation of up to 150 dB and new error sources, NCU could have comparable levels of accuracy to those of conventional quantitative ultrasound, while providing the medical and patient comfort-related advantages of not involving direct contact. [http://dx.doi.org/10.1118/1.4709598]

Key words: noncontact ultrasound, diagnostic skeletal assessment and imaging

I. INTRODUCTION AND MOTIVATION

Dual-energy x-ray absorptiometry (DXA or DEXA)[1,2] has established itself as the standard method for diagnosing osteoporosis, and it is the most widely used technique for *in vivo* measurements of bone mineral density (BMD). Other methods such as quantitative computerized tomography (QCT),[3–5] magnetic resonance imaging (MRI),[6–9] and quantitative ultrasound imaging (QUS)[10–12] have been used to make accurate measurements of bone mineral density and bone structural parameters. Although a major goal of *in vivo* bone diagnostic imaging is the accurate prediction of fracture risk, data obtained from bone research over the past two

decades suggest that factors other than bone mineral density, such as bone architecture, geometry, and microstructure, are significantly correlated to fracture risks.[13–15] The authors were motivated to develop a cortical bone ultrasound analyzer because current FDA approved ultrasound technology focuses on trabecular bone rather than cortical bone. Since most of the skeleton is cortical (80% by mass) (Ref. 16) and the majority of osteoporotic fractures originate in cortical bone,[17] the authors have pursued the development of a cortical device for quantitative ultrasound measurements. In this endeavor, they were aided by two pioneering studies that were of pivotal importance in establishing the field of ultrasonic characterization of cortical bone: the first by Tatarinov *et al.*[18] that used multiple acoustic wave modes to assess long bones, and the second by Molianen *et al.*[19] concerning the axial propagation of ultrasound in long cortical bones for use in the *in vivo* diagnosis of osteoporosis. Currently, the Hologic Sahara, Lunar Achilles, Quantitative Real-Time 2000, and CUBA Clinical systems focus on broadband ultrasound attenuation (BUA) and speed of sound (SOS) in the trabecular calcaneus, while the DBM Sonic 1200 and SoundScan 2000 devices determine the velocity of cortical bone in the phalanges and tibia, respectively.[20,21] Much of the impetus for these earlier devices was the work of Langton and collaborators[22–26] which demonstrated that a significant difference in the slope of the attenuation–frequency spectrum measured on a logarithmic scale in decibels per centimeter megahertz units (dB/cm MHz), the so-called "BUA," was a reliable index for osteoporosis. The original papers of Langton and collaborators were used to help design such devices as the Hologic Sahara which measures BUA in the trabecular calcaneus and uses this quantity to distinguish healthy from osteoporotic subjects. There are many other studies of BUA and SOS in the literature including Refs. 27–35 and two M.S. theses in biology from the California State University, Dominguez Hills Medical Physics Research Group.[36,37] Certain systems such as the SoundScan 2000 utilize axial transmission to assess skeletal status in cortical bone, whereas the authors' SIA-7 noncontact ultrasound system is similar to the Hologic Sahara and DBM 1200 Sonic and, therefore, uses transverse transmission to evaluate the quality of bone. The axial transmission method makes measurements of velocity[20] and attenuation, while transverse methods can measure velocity, attenuation, as well as BUA. In addition, the axial transmission method involves acoustical coupling gels,[20] while the noncontact method does not. Errors associated with axial transmission include uncertainties in the time of flight of the first arriving signal which implies that the signal-to-noise ratio is not optimal.[20] Although a paper by Camus states that the axial transmission technique may be applied to additional skeletal sites other than the tibia, it seems that noncontact ultrasound could potentially be applied to a greater number of skeletal sites than axial methods including conditions, sites, and procedures that involve high levels of discomfort such as contusions, burns, open wounds, the eye, recovering surgical anatomical wounds, and image guided surgery. Ultrasound speed and attenuation have been measured *in vivo* for most bodily organs and tissues over the past five decades, and *in vivo* quantitative ultrasound has been available in clinics for a similar period of time. In particular, quantitative SOS, attenuation, and BUA have been applied to osteoporosis-related diagnostics and imaging using conventional contact ultrasound. In contrast, air-coupled (noncontact) ultrasound and imaging has been available for only two decades. The assessment of the degree and extent of damage in severe burns is the only previous application of the NCU modality to medicine in the medical physics literature other than this study and related published abstracts[38] by the authors of this study. The application of NCU to burns was limited to shallow propagation into the body over small distances of a few millimeter or less.[39,40] There are small systematic errors associated with contact ultrasound including its dependence upon coupling gels and water baths, which can lead to infections[41,42] and pneumonia,[43] as a result of transducer contact and immersion. Because NCU is air-coupled, these particular errors are eliminated. In addition, NCU eliminates the minor systematic errors associated with the variable operator-dependent transducer pressure applied by a technologist.[44,45] Studies which make contact ultrasound measurements using coupling gels and water baths yield temperature-dependent results and corresponding errors.[46–49] SOS in air varies with temperature, thus NCU results are temperature-dependent as well, and the authors have taken into account this effect in the calibration procedure for the SIA-7 instrument.

This study is novel because it uses a noncontact ultrasound system to assess cortical bone phantoms. In particular, we measured SOS, integrated response (IR), and transmittance using NCU. According to the best knowledge of the authors, there are presently no published papers on the applications of NCU methods to bone assessment. Therefore, this paper would be the first to investigate the feasibility of applying noncontact ultrasound imaging and quantitative analysis to the assessment of cortical bone. This study is also novel because it involves propagation through relatively large distances in a simple and possibly routine procedure. This study generalizes and extends preliminary work conducted by one of the authors[50] on simple, trabecular bone x-ray phantoms to more realistic cortical bone phantoms specially designed for ultrasound studies of bone. The two previous papers on the clinical applications of NCU (Refs. 39 and 40) have not been followed up by additional related studies and the techniques of these early studies, which concerned classifying third degree burns, have yet to be replicated. The authors' paper is novel in that it may eventually yield the first medical application of NCU that could find significant usage in clinics.

II. MATERIALS AND METHODS

II.A. Noncontact transducers

A matched pair of piezoelectric noncontact transducers with a central frequency of 1.5 MHz and weak focusing with a radius of curvature of 0.7 m was constructed by the Ultran

System Group to the specifications of the authors of this study. The diameter of the transducers is 13 mm and the focal point was designed to be in the middle of a cylinder with the approximate dimensions of a distal radius of mean diameter of about 2.3 cm, including a soft tissue layer of about 1 cm surrounding and concentric with the distal radius. The transducers were designed to allow for separation of reflected pulses from the surfaces of the distal radius as modeled by coaxial cylinders with a 6 mm separation of inner and outer radii. Excitation pulses for the noncontact transducers are broadband chirps, which allow for the use of a synthesized pulse to help distinguish highly attenuated signal pulses from noise that has been transmitted through or reflected by the test object, usually an ultrasound phantom. Figure 1 contains an RF excitation chirp which produces a similar transmitted transducer pulse that is typical of those used in this study, while Fig. 2 contains a plot of the pulse received by the second transducer after transmission through a 9 mm polystyrene block. The frequency range of the chirp pulse from the 1.5 MHz transducers used in most of the authors' measurements contained frequencies from 1.175 to 1.925 MHz and, therefore, had a bandwidth of 0.750 MHz. The noncontact system used an amplifier with a gain that varies between 5 and 90 dB, which amounted to about 90 and 60 dB for the transmitted and reflected pulses, respectively. The amplifier is an integral component of the SIA-7 system that was designed and built by VN Instruments Ltd., Elizabethtown, ON, Canada. Figure 3 displays the results of the convolution of the received signal with a replica of the excitation pulse in a process called the synthetic impulse method patented by VN Instruments Ltd. This process is used to increase the dynamic range of the system to 150 dB, as stated in a list of the manufacturer's (the Ultran Group) specifications.[51]

II.B. Phantoms (CIRS cortical)

In order to study how changes in BMD effect the reflection and transmission of ultrasound in cortical bone *in vivo*, phantoms with calibrated amounts of hydroxyapatite, contained in a solid plastic matrix, were used to simulate human cortical bone. These rectangular shaped "bone reference plates" were constructed by Computerized Imaging Reference Systems (CIRS) of Norfolk, Virginia, from epoxy and varying concentrations of calcium hydroxyapatite, ranging from 0.0 to 1.7 g/cm^3. Therefore, the bone reference plates cover the hydroxyapatite concentration range for osteoporotic bone (BMD < 1.2 g/cm^3)[52] up to a relatively high BMD of 1.96 g/cm^3 for healthy bone.[53] The total mass density of the bone reference plates ranged from 1.15 to 1.94 g/cm^3 for the lower density phantoms that were referred to as the "BN set." The higher density set of phantoms, referred to as the "NEW set," has densities that vary from 1.82 to 2.25 g/cm^3. The dimensions of the NEW phantoms are $50 \times 50 \times 6$ mm^3. The dimensions of the BN phantoms are slightly different, $55 \times 55 \times 6$ mm^3. The BN and NEW phantoms were tested in the authors' laboratory with contact transducer frequencies of 2.25, 3.5, and 5 MHz, yielding speed of sound values that were consistent with the NCU method. The plate composed of pure plastic (with a BMD equal to zero) had the same dimensions as the other

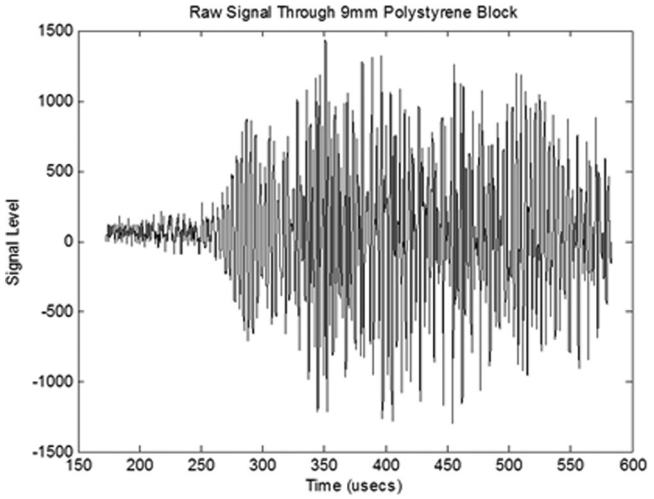

FIG. 2. A pulse received by the receiving transducer after propagation through a 9 mm block of polystyrene.

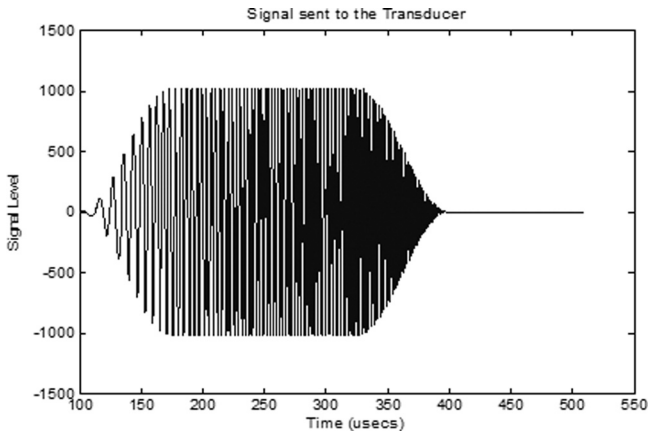

FIG. 1. A snapshot of the RF excitation pulse that was used to energize the transmitting transducer.

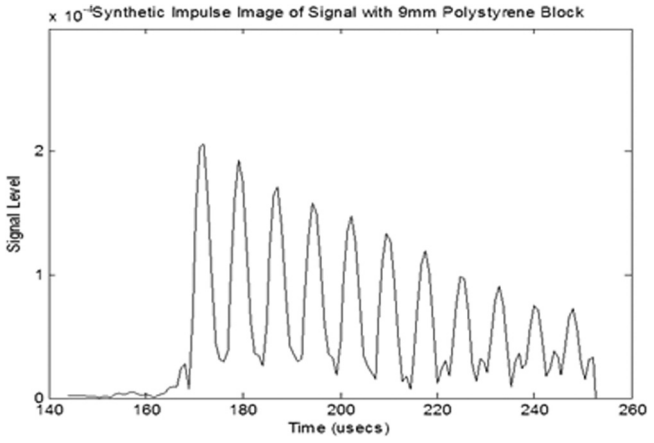

FIG. 3. A plot of the received pulse after application of the synthetic impulse method.

BN plates and a density of 1.15 g/cm^3. A representative bone phantom is shown in Fig. 4.

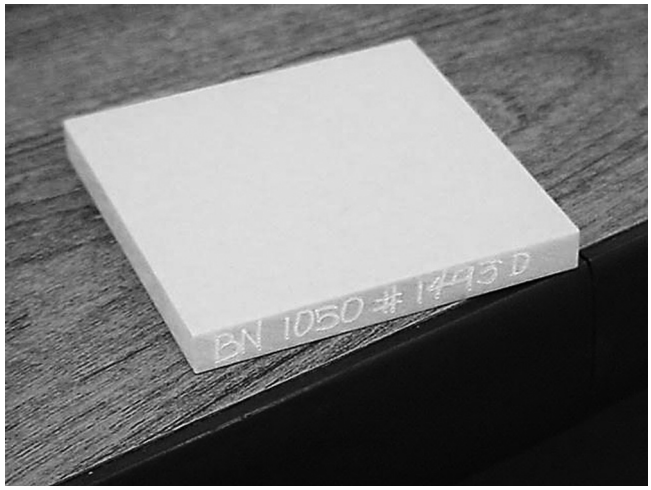

FIG. 4. One of the 17 different cortical bone phantoms from two sets, which varied in BMD from 0 to 1700 mg/cm^3.

II.C. Noncontact ultrasound methods

The analysis software–firmware combination was developed by VN Instruments Ltd. and was used to make all of the ultrasound measurements. Their ultrasound hardware consisted of two specialized noncontact transducers, a scanner from the ISEL Corporation of Eiterfeld, Germany, a pulse generator including equipment for formulating chirp pulses, a digital signal processor, a power supply, specialized software, and a computer based on a Pentium II processor running a variation of the UNIX operating system called QUNIX. A photograph of the NCU system is shown in Fig. 5. The authors' system includes a 14-bit analog to digital converter with a sampling rate of 50 MHz and 256 MB of on-board storage which sends information to a separate digital signal processing module. The SIA-7 unit consists of a digital signal processing module that includes an arbitrary function generator coupled to a digitizer. The units are locked together using a common digital clock. The waveforms are sent to a power amplifier, included as part of the system, and then received using low noise, high gain variable amplifiers which are also integral to the system. A chirp is constructed from a sine wave signal that has a linear frequency ramp applied at a precisely controlled rate. The resulting chirp signal is modulated with a stepped cosine weighting function to reduce side lobes. The chirp is used to deconvolve the received signal. The resulting image called a synthetic impulse image preserves its phase and magnitude over the entire frequency range of the transducers, amplifiers, and signals being used. Therefore, one can study synthetic impulse images in exactly the same way that researchers analyze conventional pulse-generated images. The chirp parameters can be adjusted arbitrarily and are usually setup to coincide with the gain characteristics of the transducers connected to the system, which helps to maximize the detected signals. The primary advantages of synthetic impulses are a much larger dynamic range and far greater signal stability than conventional ultrasonic methods. Such methods are commonly used in many synthetic aperture radar systems.

The SIA-7 software includes programs for interfacing and running the scanner, for signal processing, and for computing SOS, attenuation, and density for each of the four ultrasound paths (among the receiving and transmitting transducers) as illustrated in Fig. 6. The authors' NCU system uses the following technique which is significantly different from standard ultrasound methods such as a single transducer used in the pulse-echo configuration with only electronic amplifiers to determine the time of flight and attenuation relative to an initial pulse. Instead, the authors' system augments electronic amplification with the "synthetic impulse" signal processing method which performs a mathematical convolution of the received pulse with a replica of the excitation pulse to increase the overall gain beyond that obtained from standard electronic analyzers. The IR or integrated response is a numeric integration of a peak signal appearing in a synthetic impulse image.[54] The magnitude of a synthetic impulse image is proportional to the energy of the received pulse. The integrated response is an integral of a detected peak that is proportional to the total energy (in Joules) contained within a single observed peak. The proportionality constant is not known but the relative signals can be used to compute ratios including transmission and reflection coefficients. The speed of sound is computed using a centroid method. The time of flight for a single peak is measured by fitting a third order polynomial to an observed peak and locating the local maximum associated with the peak. This technique allows for a larger signal-to-noise level with a larger dynamic range than that obtained from the received pulse alone. This approach allows for detection of very weak signals and more accurate measurements of the transmission, IR, and SOS than that of standard ultrasound. The authors note that the synthetic impulse approach resembles matched-filtering methods that are frequently used to process electromagnetic signals in

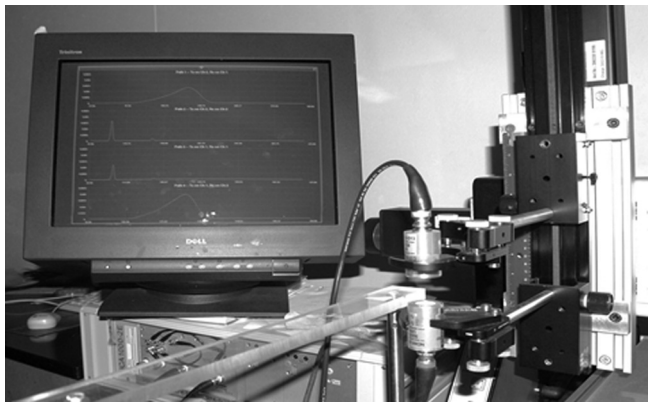

FIG. 5. The NCU measurement configuration showing the upper and lower transducers, the monitor screen, the scanning system, and the computer software utilized to measure the SOS, IR, attenuation, and thickness for all of the cortical bone phantoms.

contemporary remote sensing systems such as those involving radar.

A careful mechanical alignment of the transducers is undertaken, when needed, by maximizing the peak value of the IR and the number of observable peaks in the two reflection paths called P2 (back scattering from the lower transducer) and P3 (back scattering from the upper transducer), as displayed in Fig. 6. This optimization process involves slightly tilting each transducer by using three adjustable springs. When studying the speed, thickness, and time of flight in a calibration block designed for the authors' transducers provided by the manufacturer, a systematic realignment was performed about once every 2 weeks or when there was some indication that the system's alignment had been significantly changed. The authors estimate that a proper alignment involves relative tilts of the transducers of less than approximately 3°. After the alignment was completed, the authors performed a calibration procedure that was built into the system, which involved measuring the SOS in the air between the transducers, using adjustments of the expected SOS based on small variations of the nominal SOS in air due to the ambient temperature and possibly other environmental factors such as humidity. The air calibration was followed by a similar calibration with the sample in place and a quality control (QC) procedure on a test block that was part of the system, as recommended by the manufacturer. After these basic measurements were undertaken, the authors used the calibrated system to make measurements on each of the 17 rectangular cortical bone phantoms (Fig. 4) to determine SOS, thickness, time of flight, and IR for each phantom. Most of the data presented in this study were collected from these bone phantoms. A group of test objects similar to the authors' cortical bone phantoms might be a useful tool for calibrating some future NCU system to measure bone mechanical properties in a clinical setting.

II.D. The scanning system

The authors' scanning system has the capability to perform two-dimensional (2D) ultrasound scans over an array of square shaped pixels with dimensions as small as 0.1 mm $\times$ 0.1 mm. The duration of a scan that is capable of producing a clear image can be as short as 2–5 min and as long as about 30 min and is dependent upon the pulse-repetition frequency (PRF). If a phased array of NCU transducers were available for usage with the Second Wave/VN Instruments Ltd. analyzer, it could be employed to measure depth and undertake a 3D scan of an array of voxels.

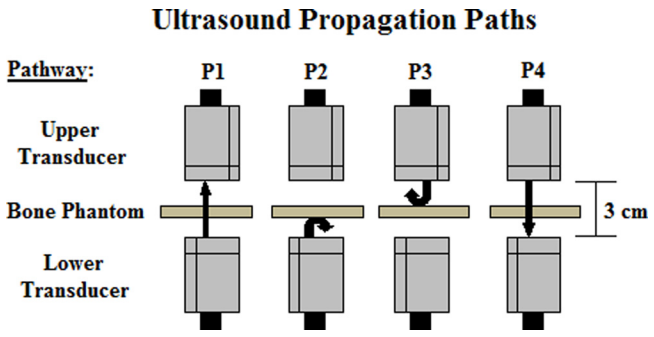

FIG. 6. The velocity/thickness algorithm uses measurements of the time of flight and signal strength in these four propagation paths. P1 and P4 are the two transmission paths and P2 and P3 represent the two reflection paths.

II.E. Mechanism for the SOS measurements

The vertical position of the horizontally aligned transducers relative to each other and to the sample changed from experiment to experiment, but the exact position was always known from the set-up calibration procedure. The time of flight of transmitted pulses was measured without a sample between the transducers and then multiplied by the SOS value in air to obtain an accurate value for the distance between the transducers, which was automatically calculated by the signal processor. The central plane of the sample usually bisected the distance between the two transducers which were approximately separated by a total distance of 3.0 cm; however, the exact position was obtained from the time-of-flight measurements of the first reflection peak for both paths, P2 (bottom surface) and P3 (top surface).

III. RESULTS

The values of the SOS measurements using contact ultrasound ranged from approximately 2450–3090 m/s. To be specific, the measured SOS is the group velocity of the pulse through the sample. Since the phase velocity is constant over the band of frequencies that travel through the phantom, the group and phase velocities are equivalent in this case and there is no dispersion in the samples. NCU measurements of SOS on the cortical phantoms as a function of density were conducted repeatedly over $2\frac{1}{2}$ yrs. and the results of these measurements are displayed in Fig. 7. A conspicuous characteristic of this figure is the monotonic increase in SOS with phantom density, which is in agreement with a previous study by Yamato *et al.*[55] that demonstrates that SOS is directly proportional to density. The physical mechanism behind the steady increase in SOS is due to the fact that the material becomes more closely packed (with higher density and compressibility) and rigid, and as the elastic modulus, which is dependent on the mineral density,[56] increases, the speed, acoustical absorption, and attenuation increase as well. Figure 7 compares the authors' results to similar contact measurements and demonstrates that the SOS values obtained using the authors' noncontact methods are almost identical to those taken with their standard, single transducer, pulse-echo contact technique. The close agreement in the data for the two techniques provides a validation for the usage of NCU, demonstrating that any new sources of systematic errors specific to NCU are likely small in the authors' measurements. Figure 7 displays SOS results for the full range of samples from the two sets of phantoms studied, which spans the full range of bone mineral densities found *in vivo* for healthy adults as well as those with osteoporosis. The values of the phantom densities and SOS in NCU resulted in acoustical impedances of the phantoms ranging from 2.79 to 6.89 $\times$ 10^6 kg/(m^2·s),

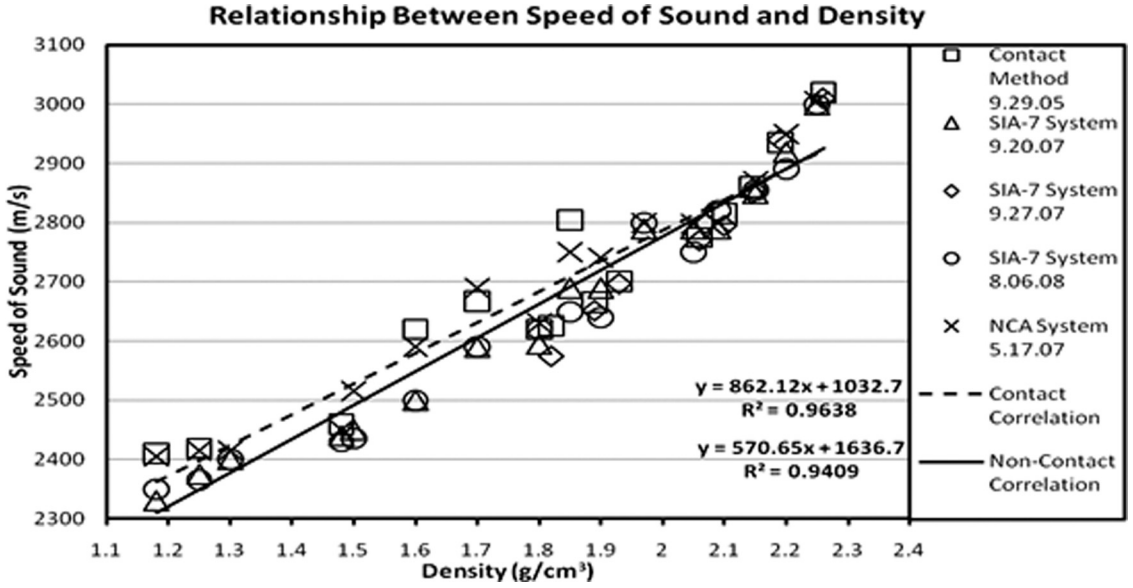

FIG. 7. Measurements of SOS as a function of density comparing the data collected from conventional contact ultrasound by using the single transducer pulse-echo technique with data collected from the authors' SIA-7 and NCA-1000 noncontact analysis programs with their NCU analyzer. Both programs were used to collect data from the BN and NEW phantom sets during the dates noted in the legend, on the right.

where the higher value corresponds to about 97% of the average *in vivo* value of the acoustical impedance in cortical bone.[57] In addition, the authors found that their SOS data were consistent and reproducible over a $2^1/_2$ yr period, providing additional confirmation of the stability of NCU measurements and commensurability with conventional contact ultrasound.

The reproducibility of SOS measurements for a given sample (one from each set of phantoms) was studied by making similar measurements over an extended period of time. A second indicator of the reproducibility and reliability of the NCU method was obtained through repeated measurements of the thickness of each of the phantoms in the two phantom sets. Sixteen repeated measurements ($n = 16$) of SOS on the NEW 1400 mg/cc as well as twenty measurements ($n = 20$) of SOS in the BN 750 mg/cc phantoms yielded means and standard deviations equal to 2832.1 and $\sigma = 50.4$ m/s (1.8%) and 2562.2 m/s and $\sigma = 33.4$ m/s (1.3%), respectively. The 1.3% error in the authors' SOS measurements is relatively high in comparison to similar measurements using contact ultrasound. This increased error in NCU is likely due to such sources as turbulence and nonuniformity in the density from pixel to pixel across the surface of the sample. Temperature variations in the air gaps resulting in changes in the SOS in air is probably the most significant source of error and other sources of uncertainties include turbulence and currents in the air gaps that could be limited in follow-up studies through the usage of a plastic enclosure as a wind shield. In addition to SOS, 16 repeated measurements ($n = 16$) of phantom thickness for the NEW 1400 mg/cc as well as 20 measurements ($n = 20$) of thickness for the BN 750 mg/cc phantom yielded means and standard deviations equal to 6.15 mm and $\sigma = 0.029$ mm (0.4%) and 5.96 mm and $\sigma = 0.026$ mm (0.4%), respectively.

The IR is a measure of the total power of the signal. It is equal to the area or integral under the first peak in the transmitted pulse, with units of decibel-seconds. Transmission is a measure of the fraction of the ulrasound energy that is transferred directly (without reflections) through the sample. By Parseval's theorem, the integral of the square of a function is equal to the integral of the square of its Fourier transform.[58] As indicated in Figs. 8(a) and 8(b), the fraction of the signal that passes through the sample decreases as the density increases, in a nearly uniform manner. A portion of the decrease in IR as a function of BMD is due to the increasing impedance mismatch at the two air–sample interfaces. As the difference in acoustical impedance increases, the intensity of the reflected pulse (R) increases, and thus the transmitted intensity (T) decreases, since $R + T = 1$ (with proper normalization), by virtue of conservation of energy.

A prominent feature in Figs. 8(a) and 8(b) is the constant diplacement of the two linear curves representing the two different analysis protocols (NCA-1000 and SIA-7) which have nearly the same slope but a different IR intercept, indicating an offset by a constant number of decibels. The intercept of the IR curves are -10 and -100 dB for the NCA-100 and SIA-7 systems, respectively. This significant difference is due to a corresponding difference in the choice of the standard voltage ($V_{standard}$). Therefore, the only difference between the two protocols is a constant number of decibels which is related to a corresponding difference in the standard voltage. The measured attenuation (in decibels) is defined by the following well-known expression: $A(dB) = 20 \log_{10} (V/V_{standard})$. Langton *et al.*[59] and Sasso *et al.*[60] both studied the dependence of BUA on BMD using conventions that differ by a multiplicative minus sign and an additive constant. The authors' data for the IR parameter are similar to the data on BUA published by Sasso, in that both the authors' IR and Sasso's BUA data are inversely proportional to BMD. As suggested above, the slope calculated from a linear fit to the A (db) versus density ρ (g/cm^3) plot [$S = \Delta A(dB)/(\Delta\rho$(g/

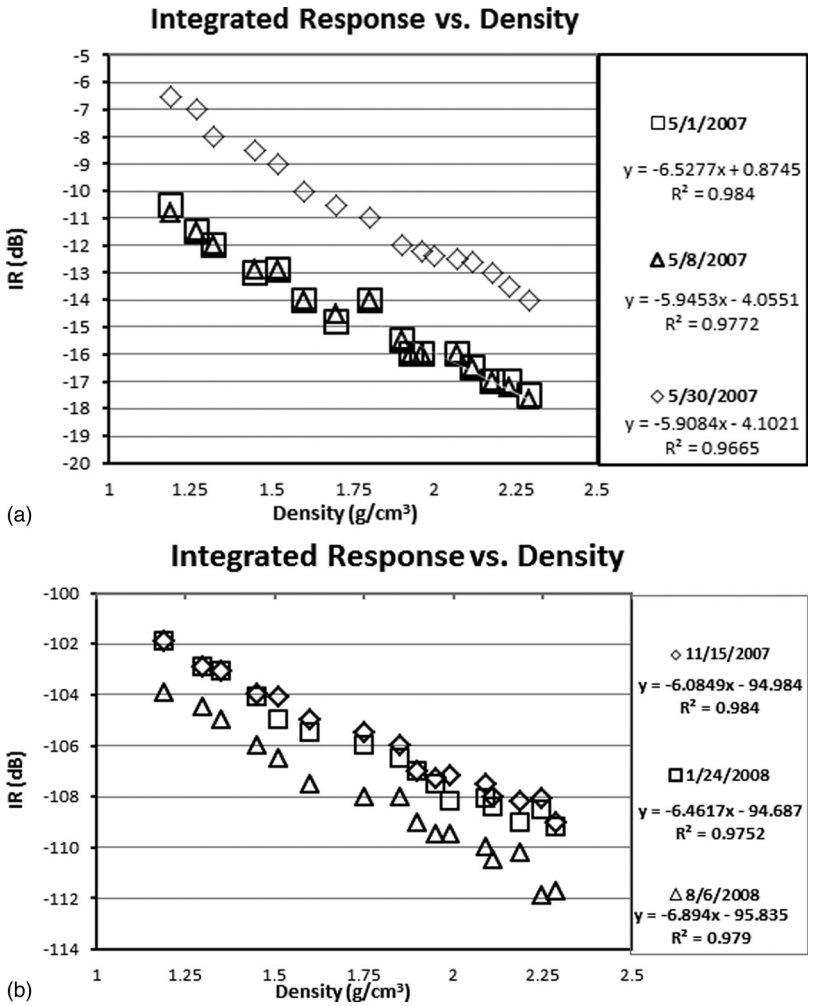

FIG. 8. (a) IR as a function of phantom density using the NCA-1000 and Pathway 4 (P4) which is used for pulses that are emitted from the upper transducer, transmitted through the sample, and received by the lower transducer. (b) IR as a function of phantom density measured using the SIA-7 protocol for the same pathway as in (a).

cm^3)] is similar in both protocols. Linear regressions for the three curves in both Figs. 8(a) and 8(b) yield similar average slope $[S = \Delta A(dB)/(\Delta\rho\ (g/cm^3)]$ values of -6.509 and -6.668 for the NCA-1000 and SIA-7 analyses, respectively, which yield a small difference of less than 2.5%.

In Fig. 9, a third noncontact ultrasound parameter, the transmittance of the acoustical signal through the sample (T), was used to formulate images of some of the cortical bone phantoms as a function of density. These images were created using a color scale to construct a visually perceptible representation of the transmittance as a function of BMD. Figure 9 suggest a linear proportionality between transmittance and BMD. The color scale was configured such that transmittance increases with the visible-light wavelength (from blue to red). The IPass images clearly demonstrate that transmittance decreases as BMD increases. The images in Fig. 9, which include only the BN phantom set, are all standardized relative to the BN 300 phantom, and the pixel-averaged transmittance for both phantom sets are plotted in Fig. 10.

C-line scan averages were determined for each phantom from a horizontal line drawn across the diameter of the sample by averaging the peak-to-peak transmittance amplitude in millivolts over all the pixels on the line. The resulting averages are plotted versus density in Fig. 10, which exhibits a very strong linear relationship between the density of the sample and its transmittance.

Statistical and systematic errors are used to determine the values of the accuracy and precision errors. Possible sources of these errors related to propagation through the air are the temperature, properties of air currents, humidity, barometric pressure, and turbulence. Sources of errors in the signal-to-noise ratio include imperfect acoustical alignment, wave acoustical effects such as diffraction and interference, and the specifications and performance of the pulse generator, detector, digitizer, signal processor, and electronic noise. Systematic errors associated with system hardware also include the seven parameters used to define the transducer excitation chirp, the central frequency, and the bandwidth of the transducers; the configuration, geometry, and uniformity of the phantoms (including alignment, tilts, and nonuniformities), and the calibration stability. Possible sources of errors in the software are associated with the stability of the time offsets, signal processing, pulse averaging, and the stability of the interface between the scanner and the analysis system.

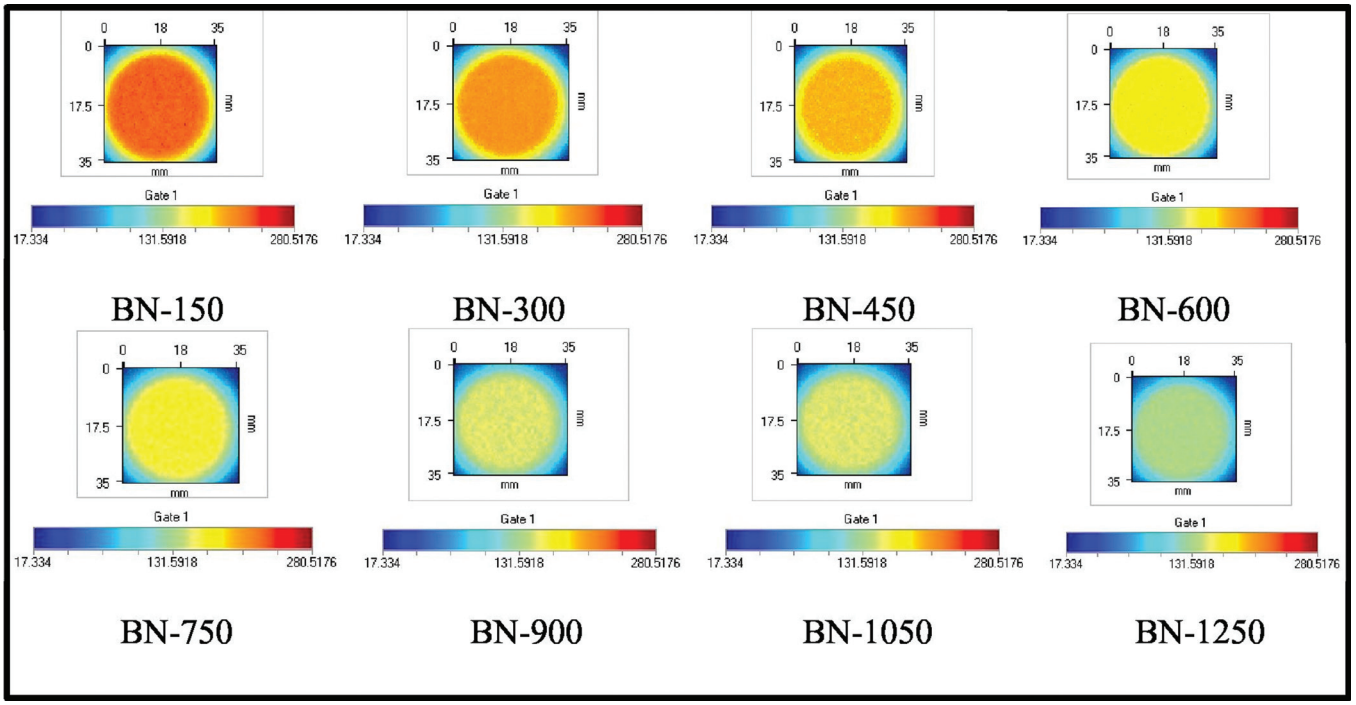

FIG. 9. Transmittance images of the cortical bone phantoms using the IPass system. The BMD ranges from 150 to 1250 mg/cm^3.

IV. DISCUSSION AND CONCLUSIONS

The authors' results show that noncontact measurements of the speed of sound, integrated response, and transmittance are directly or inversely proportional to the mass density of the cortical bone phantoms. Therefore, future *in vivo* studies of NCU might be able to accurately determine bone mineral density, and ultimately ultrasound could possibly be used to undertake bone diagnostics in clinics to supplement data obtained using radiological techniques such as DXA and QCT.

The authors plan to perform more detailed experiments on phantoms including those involving skin-simulating materials to augment the bone phantom data obtained in this study, including attenuation and spectroscopic measurements. In the long term, they foresee that NCU research will involve cadaver studies for calibration and validation, as well as clinical trials with human subjects for use in the diagnosis and monitoring of osteoporosis. This study takes a first step in that direction by demonstrating that standard clinical ultrasound measurements conducted with noncontact ultrasound can agree well with those of contact ultrasound and, therefore, might be adapted to a clinical setting. The results are highly reproducible over time and under variable conditions. These results also demonstrate that an NCU system, correctly configured and calibrated, can have a level of reproducibility and reliability for quantitative measurements that is comparable to conventional contact ultrasound, despite the additional high level of attenuation due to propagation through air and large acoustical impedance mismatches at the interfaces resulting in large losses due to reflection.

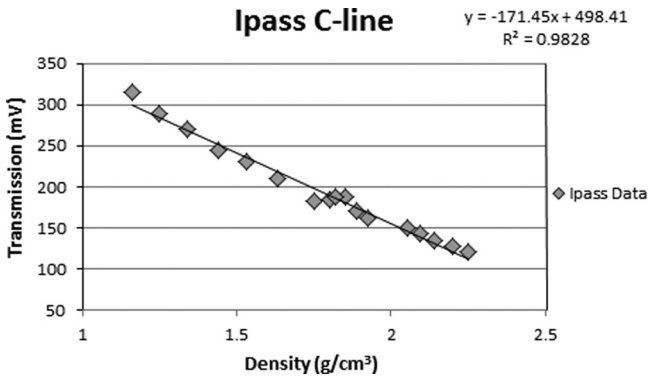

FIG. 10. Average transmittance of the IPass C-scans as a function of phantom density for both phantom sets. A least-squares line fit is included and plotted.

Since the authors' current system already has a suitable geometric configuration, they intend to make scans of the hand *in vivo*, in particular to scan the phalanges to determine SOS, thickness, time of flight, IR, attenuation, and BUA that might be useful for skeletal imaging and bone diagnostics. Similar studies have been undertaken on the phalanges in a clinical study using conventional contact ultrasound as in a relatively recent paper by Guglielmi *et al.*[61] that showed promise for clinical usage. In follow-up papers, the authors hope to apply the NCU technique to the phalanges, therefore, using the advantages in convenience, safety (by avoiding ultrasound gels as well as ionizing radiation), accuracy (through minimization of systematic errors), reproducibility through the lack of reliance on pressure-dependent transducers applied by an ultrasound technologist,[44,45] and the availability of position-accurate, repeatable scans that could be provided by using preprogrammed software and a precision scanner along with an NCU system. NCU signals are highly attenuated because impedance mismatches imply

74 dB losses due to two transmissions through surfaces between air and cortical bone. Given recent concerns over risks due to exposure to ionizing radiation in radiological imaging and the low level of patient risks involved in ultrasound imaging, NCU might find a clinical niche if developed in the near future. Longstanding high prevalence rates of serious osteoporotic fractures at such sites as the femoral neck, the hip, and the spine especially among the aged,[62] provide an additional impetus to develop NCU in the near term for the purpose of skeletal diagnostics. Quantitative ultrasound measurements using NCU might avoid some of the systematic errors found in conventional contact QUS imaging due to its lack of operator intervention or coupling gels, thus eliminating the risk of allergic reactions to the gel as well as the discomfort and inconvenience of the gels. As mentioned in the Introduction, NCU imaging may also be useful for performing ultrasound examinations in situations where contact ultrasound might be highly painful, uncomfortable, or harmful as in the case of imaging of the eyes or in the assessment of severe burns and other serious wounds.

ACKNOWLEDGMENTS

The authors would like to express their gratitude to the National Institutes of Health who supported this research through Grant No. GM 08156-22 and its supplements which included funding for obtaining an NCU system and other ultrasound hardware used in this study. The authors greatly appreciate the expert assistance provided by Dr. Mahesh Bhardwaj and Mr. Michael Biviano of the Ultran Group.

[a]Electronic mail: kganezer@csudh.edu

[1]P. Tothill, "Methods of bone mineral measurement," Phys. Med. Biol. **34**, 543–572 (1989).
[2]M. A. Greenfield, "Current status of physical measurements of the skeleton," Med. Phys. **19**, 1349–1357 (1992).
[3]T. N. Hangartner and D. F. Short, "Accurate quantification of width and density of bone structures by computed tomography," Med. Phys. **37**, 3777–3784 (2007).
[4]P. M. Joseph and C. Ruth, "A method for simultaneous correction of spectrum hardening artifacts in CT images containing both bone and iodine," Med. Phys. **24**, 1629–1634 (1997).
[5]M. M. Goodsitt, "Beam hardening errors in post-processing dual energy quantitative computed tomography," Med. Phys. **22**, 1039–1047 (1995).
[6]S. Majumdar, H. K. Genant, S. Grampp, D. C. Newitt, V. H. Truong, J. C. Lin, and A. Mathur, "Correlation of trabecular bone structure with age, bone mineral density, and osteoporotic status: *In vivo* studies in the distal radius using high resolution magnetic resonance imaging," J. Bone Miner. Res. **12**, 111–118 (1997).
[7]F. W. Wehrli, S. N. Hwang, J. Ma, H. K. Song, J. C. Ford, and J. G. Haddad, "Cancellous bone volume and structure in the forearm: Noninvasive assessment with MR microimaging and image processing," Radiology **206**, 347–357 (1998).
[8]M. Wessels, R. P. Mason, P. P. Antich, J. E. Zerwekh, and C. Y. C. Pak, "Connectivity in human cancellous bone by three-dimensional magnetic resonance microscopy," Med. Phys. **24**, 1409–1420 (1997).
[9]J. Blumenfield, C. Studholma, J. Carballido-Gamio, D. Carpenter, T. M. Link, and S. Majumdar, "Three-dimensional image registration of MR proximal femur images for the analysis of trabecular bone parameters," Med. Phys. **35**, 4630–4639 (2008).
[10]C. M. Langton, C. F. Njeh, R. Hodgkinson, and J. D. Currey, "Predictions of mechanical properties of the human calcaneus by broadband ultrasonic attenuation," Bone **18**,495–503 (1996).
[11]R. Hodgkinson, C. F. Njeh, M. A. Whitehead, and C. M. Langton, "The non-linear relationship Between BUA and porosity in cancellous bone," Phys. Med. Biol. **41**, 2411–2420 (1996).
[12]M. L. McKelvie and S. B. Palmer, "The interaction of ultrasound with cancellous bone," Phys. Med. Biol. **36**, 1331–1340 (1991).
[13]T. J. Beck, A. C Looker, F. Mourtada, M. M. Daphtary, and C. B. Ruff, "Age trends in femur stresses from a simulated fall on the hip among men and women: Evidence of homeostatic adaptation underlying the decline in hip BMD," J. Bone Miner. Res. **21**(9), 1425–1432 (2006).
[14]J. G. Snedeker, F. H. Walz, M. H. Muser, G. Schroeder, T. L. Mueller, and R. Müller, "Microstructural insight into pedestrian pelvic fracture as assessed by high-resolution computed tomography," J. Biomech. **39**(14), 2709–2713 (2006).
[15]R. O. Ritchie, M. J. Buehler, and P. Hansma, "Plasticity and toughness in bone," Phys. Today **62**(6), 41–47 (2009).
[16]J. L. Ferretti *et al.*, "Perspectives: On osteoporosis research: Its focus and some insight of a new paradigm," Calcif. Tissue Int. **57**, 399–404 (1995).
[17]E. Camus, "Analysis of the axial transmission technique for the assessment of skeletal status," J. Acoust. Soc. Am. **108**, 3058–3064 (2000).
[18]E. Tatarinov, N. Sarvazyan, and A. Sarvazyan, "Use of multiple acoustic wave modes for assessment of long bones: Model study," Ultrasonics **43**, 672–680 (2005).
[19]P. Molianen, V. Kilappa, P. H. F. Nicholson, J. Timonen, and S. Cheng, "Thickness sensitivity of ultrasound velocity in long bone phantoms," Ultrasound Med. Biol. **30**(11), 1517–1521 (2004).
[20]C. F. Njeh, C. M. Bovin, and C. M. Langton, "The role of ultrasound in the assessment of osteoporosis: A review," Osteoporosis Int. **7**, 7–22 (1997).
[21]J. J. Kaufman, G. M. Luo, D. Conroy, W. A. Johnson, R. L. Altman, and R. S. Siffert, "New ultrasound system for bone assessment," Proc. SPIE **5373**, 212–222 (2004).
[22]C. M. Langton, "Critical analysis of the ultrasonic interrogation of bone and future developments," in *Ultrasonic Studies of Bone*, edited by S. P. Palmer and C. M. Langton (IOP, Bristol, 1987), pp. 73–89.
[23]C. M. Langton, "The role of ultrasound in the assessment of osteoporosis," Clin. Rheumatol. **13**(S1), 13–17 (1994).
[24]C. M. Langton *et al.*, "A contact method for the assessment of ultrasonic velocity and broadband attenuation in cortical and cancellous bone," Clin. Phys. Physiol. Meas. **11**(3), 243–249 (1990).
[25]R. Hodgskinson, C. F. Njeh., M. A. Whitehead, and C. M. Langton, "The non-linear relationship between BUA and porosity in cancellous bone," Phys. Med. Biol. **41**, 2411–2420 (1996).
[26]P. H. F. Nicholson, G. Lowet, C. M. Langton, J. Dequeker, and G. Van der Perre, "A comparison of time-domain and frequency-domain approaches to ultrasonic velocity measurement in trabecular bone," Phys. Med. Biol. **41**, 2421–2435 (1996).
[27]C. M. Langton, C. F. Njeh, R. Hodgkinson, and J. D. Currey, "Predictions of mechanical properties of the human calcaneous by broadband ultrasonic attenuation," Bone **18**, 495–503 (1996).
[28]R. Hodgkinson, C. F. Njeh, M. A. Whitehead, and C. M. Langton, "The non-linear relationship between BUA and porosity in cancellous bone," Phys. Med. Biol. **41**, 2411–2420 (1996).
[29]M. L. McKelvie and S. B. Palmer, "The interaction of ultrasound with cancellous bone," Phys. Med. Biol. **36**, 1331–1340 (1991).
[30]R. Strelitzki, A. J. Clarke, and J. A. Evans, "The measurement of the velocity of ultrasound in fixed trabecular bone using broadband pulses and single-frequency tone bursts," Phys. Med. Biol. **41**, 743–753 (1996).
[31]P. Antich and S. Mehta, "Ultrasound critical-angle reflectometry: A new modality for functional elastometric imaging," Phys. Med. Biol. **42**(9), 1763–1777 (1997).
[32]C. M. Langton, M. A. Whitehead, T. J. Haire, and R. Hodgskinson, "Fractal dimension predicts broadband ultrasound attenuation in stereo lithography models of cancellous bone," Phys. Med. Biol. **43**(2), 467–471 (1998).
[33]L. H. Le, "An investigation of pulse timing techniques for broadband ultrasonic velocity determination in cancellous bone: A simulation study," Phys. Med. Biol. **43**(8), 2295–2308 (1998).
[34]S. M. Han and J. Davis, "A comparison between the patella and the calcaneous using ultrasound velocity and attenuation as predictors of bone mineral density," Phys. Med. Biol. **42**(10), 1947–1955 (1997).
[35]R. Mazess, J. Trempe, T. Genske, and S. Wiener, "Ultrasound measurement of the os calcis," in *Current Research in Osteoporosis and Bone Mineral Measurements II: 1992, Bath, England*, edited by E. F. G. Ring (British Institute of Radiology, London, 1992).

[36]J. N. Yano, "Correlation analysis of the speed and attenuation of ultrasonic pulses with physical and radiological parameters as an assessment for bone strength and quality," M.S. thesis, CSU Dominguez Hills, Spring, University Microfilms, Ann Arbor, Michigan, UMI number 1384243, 1997.
[37]K. L. Hurst, "Ultrasound analysis of cortical bone model: New method for early detection of osteoporosis," M.S. thesis, CSU Dominguez Hills, summer, University Microfilms, Ann Arbor Michigan, 2003.
[38]J. Bulman and K. Ganezer, "Non-contact ultrasound imaging applied to cortical bone phantoms for determination of bone mineral density, speed of sound, and ultrasound attenuation," Med. Phys. **36**, 2437 (2009).
[39]J. P. Jones, D. Lee, M. Bhardwaj, V. Vanderkam, and B. Achauer, "Non-contact ultrasonic imaging for the evaluation of burn-depth and other biomedical application," Acoust. Imaging **23**, 89–93 (1997).
[40]S. Iraniha, M. E. Cinat, V. Vanderkam, A. Boyko, D. Lee, J. P. Jones, and B. M. Achauer, "Burn depth with non-contact ultrasonography," J. Burn Care Rehabil. **21**, 333–338 (2000).
[41]J. Hutchinson, W. Runge, M. Mulvey, G. Norris, M. Yetman, N. Valkova, R. Villemur, and F. Lepine, "Burkholderia cepacia infections associated with intrinsically contaminated ultrasound gel: The role of microbial degradation of parabens," Infect. Control Hosp. Epidemiol. **25**, 291–296 (2004).
[42]K. Weist, C. Wendt, L. Peterson, H. Versmold, and H. Ruden, "An outbreak of pyodermas among neonates caused by ultrasound gel contaminated with methicillin-susceptible Staphylococcus aereus," Infect. Control Hosp. Epidemiol. **21**, 761–764 (2000).
[43]O. Gaillot, C. Marue'jouls, E. Abachin, F. Lecuru, G. Arlet, M. Simonet, and P. Berche, "Nosocomial outbreak of Klebsiella pneumonia producing SHV-5 extended-spectrum β-lactamase, originating from a contaminated ultrasonography coupling gel," J. Clin. Microbiol. **36**, 1357–1360 (1998).
[44]T. B. Brismar, "MR relaxometry of lumbar spine, hip, and calcaneus in healthy premenopausal women: Relationship with dual energy x-ray absorptiometry and quantitative ultrasound," Eur. Radiol. **10**, 1215–1221 (2000).
[45]F. E. Alanfeld, C. Wuster, C. Funck, J. F. S. Pereira-Lima, T. Fritz, P. J. Meeder, and R. Ziegler, "Ultrasound measurements at the proximal phalanges in healthy women and patients with hip fractures," Osteoporosis Int. **8**, 393–398 (1998).
[46]N. A. Pocock, A. Babichev, N. Culton, K. Graney, J. Rooney, D. Bell, and J. Chu, "Temperature dependency of quantitative ultrasound," Osteoporosis Int. **11**, 316–320 (2000).
[47]F. G. Evans, "Mechanical properties and histology of cortical bone from younger and older men," Anat. Rec. **81**, 1–11 (1976).
[48]M. A. Paggiosi, A. Blumsohn, R. Barkmann, and R. Eastell, "Effect of temperature on the longitudinal variability of quantitative ultrasound variables," J. Clin. Densitom. **8**, 436–444 (2005).
[49]C. Chappard, G. Berger, C. Roux, and P. Laugier, "Ultrasound measurement on the calcaneus: Influence of immersion time and rotation of foot," Osteoporosis Int. **9**, 318–326 (1999).
[50]K. S. Ganezer, K. Hurst, S. Shukla, R. Sinow, and M. Bhardwaj, "Initial studies of non-contact ultrasound for osteoporosis and bone imaging," *American Association of Physicists in Medicine(AAPM) 44th Annual Meeting, Oral Presentation MO-D-519-3*, Montreal Quebec, Canada, July 2002; Med. Phys. **29**(6), 1292 (2002).
[51]G. Busse, G. Busse, D. V. Hemelrijck, and I. Solodov, *Emerging Technologies in Non-Destructive Testing* (Taylor & Francis, Stuttgart, Germany, 2008).
[52]Y. Duan, C. H. Turner, B. Kim, and E. Seeman, "Sexual dimorphism in vertebral fragility is more the result of gender differences in age-related bone gain than bone loss," J. Bone Miner. Res. **16**, 2267–2275 (2001).
[53]A. L. Huddleston, "A model for the *in-vivo* assessment of bone strength," Ph.D. dissertation, UCLA, 1976, University Microfilms, Ann Arbor, Michigan, UMI number 48106, 1976.
[54]I. M. Hallaj, "Ultrasonic testing using synthetic impulses," J. Acoust. Soc. Am. (Reviews of Acoustical Patents) **114**(6), Part 1, 2981 (2003).
[55]Y. Yamato, M. Matsukawa, T. Otani, K. Yamazaki, and A. Nagano, "Distribution of longitudinal wave properties in bovine cortical bone *in vitro*," Ultrasonics **44**, 233–237 (2006).
[56]D. R. Carter and W. C. Hayes, "The compressive behavior of bone as a two-porous structure," J. Bone Jt. Surg. Am. **59**, 954–962 (1977).
[57]A. Meunier, J. L. Katz, P. Christel, and L. Sedel, "A reflection scanning acoustic microscope for bone and bone-biomaterials interface studies," J. Orthop. Res. **6**, 770–775 (1988).
[58]K. F. Riley and M. P. Hobson, *Essential Mathematical Methods for the Physical Sciences* (Cambridge University Press, New York, 2011).
[59]C. M. Langton, S. B. Palmer, and R. W. Porter, "The measurement of broadband ultrasonic attenuation in cancellous bone," Eng. Med. **13**, 89–91 (1984).
[60]M. Sasso, G. Haiat, Y. Yamato, S. Naili, and M. Matsukawa, "Dependence of ultrasonic attenuation on bone mass and microstructure in bovine cortical bone," J. Biomech. **41**, 347–355 (2008).
[61]G. Guglielmi, C. F. Njeh, F. de Terlizzi, D. A. De Serio, A. Scillitani, M. Cammisa, B. Fan, Y. Lu, and H. K. Genant, "Phalangeal quantitative ultrasound, phalangeal morphometric variables, and vertebral fracture discrimination," Calcif. Tissue Int. **72**, 469–477 (2003).
[62]A. C. Looker, E. S. Orwoll, C. Conrad, J. R. Johnston, R. L. Lindsay, H. W. Wahner, W. L. Dunn, M. S. Calvo, T. B. Harris, and S. P. Heyse, "Prevalence of low femoral bone density in older U.S. adults from NHANES III," J. Bone Miner. Res. **12**, 1761–1768 (1997).